Cluster-configuration-interaction analysis of Cu $2p$ and valence-band photoemission measurements on $Bi_2Sr_2CaCu_2O_8$ and $Bi_2Sr_2CuO_6$ superconductors

G. Chiaia, M. Qvarford, and I. Lindau

Department of Synchrotron Radiation Research, Institute of Physics, Lund Unviersity, Sölvegatan 14, S-22362 Lund, Sweden

S. Söderholm, U. O. Karlsson, and S. A. Flodström

Materials Physics, Department of Physics, Royal Institute of Technology, S-10044 Stockholm, Sweden

L. Leonyuk

Moscow State University, Department of Geology, 119 899 Moscow, Russia

A. Nilsson and N. Mårtensson

Department of Physics, Uppsala University, Box 530, S-75121 Uppsala, Sweden

The electronic structure of $Bi_2Sr_2CaCu_2O_8$ and $Bi_2Sr_2CuO_6$ high-T_c superconductors is investigated by Cu $2p$ x-ray photoemission spectroscopy and valence-band resonant photoemission at the Cu L_3 edge. The data suggest strong correlation effects for the Cu $3d$ electron states due to a large on-site Coulomb interaction. By means of a simplified cluster-configuration-interaction model we derive the model Hamiltonian parameters which quantify the Cu d-d interaction energy, the O to Cu charge-transfer energy, and the degree of Cu d–O $2p$ hybridization. The solutions for the two compounds differ mainly in the charge-transfer energy, which in both cases is lower than the energy required for a Cu d-d charge fluctuation. An energy gap of about 1 eV for both compounds is found. This identifies them as charge-transfer insulators, in analogy with what was already found for CuO and other copper oxide based high-T_c superconductors. The density of states at the Fermi level is assigned to doping induced states in the semiconductor gap.

I. INTRODUCTION

Core-level photoemission measurements on CuO (Ref. 1) and on high-T_c superconductors[2] (HTS's) containing copper oxide layers, give clear evidence of strong correlation effects resulting in the presence of an intense satellite in each term of the Cu $2p$ spin-orbit doublet.

Among the earliest works on copper and nickel compounds, the first step toward a quantitative interpretation of the core-level spectra was made by Larsson.[3] His work could explain, by means of a simplified configuration-interaction approach, the presence of strong satellites resulting from the interaction between the created core hole and the valence electrons. In this approach, the initial and final states in the photoemission process are expanded on different electronic configuration basis sets. By applying the same model, the energy position and multiplet structure of the satellite in the Cu $2p$ X-ray photoemission spectroscopy (XPS) spectra of copper dihalides has been related to the screening charge-transfer process from the ligand to the metal ions.[4] Within this framework many spectroscopic properties can be evaluated as a function of a few model parameters: the charge-transfer energy Δ, the ligand-p–metal-d hybridization energy T, and the d-d Coulomb repulsion energy U involved in the charge fluctuation between two neighbor metal ions.

This model was later extended to nickel dihalides,[5] and

a comparison between the Anderson Hamiltonian—single impurity approach and a single cluster approximation—configuration-interaction approach has been drawn. This comparison shows that the configuration-interaction-cluster model is a good approximation to the full impurity-type calculation in the case of highly correlated compounds.

Cluster model calculation proved to be particularly suitable for the determination of the electronic structure of transition-metal oxides[6,7] and HTS compounds.[8] In these investigations the insulating or metallic behavior of the studied compounds has been interpreted within the systematic given by Zaanen, Sawatzky, and Allen.[9]

A simplified cluster model has been recently exploited to study some layered copper oxide superconductors[2] belonging to the La-Sr-Cu-O and Y-Ba-Cu-O families. We have applied the same model to study the electronic structure of two compounds belonging to the Bi-Sr-Ca-Cu-O family: $Bi_2Sr_2CaCu_2O_8$ (Bi2212) and $Bi_2Sr_2CuO_6$ (Bi2201). In this approach multiplet and crystal-field splittings are neglected, thus all the electronic configurations with the same $3d$ occupation number are degenerate in energy and represented by a single δ-like energy level.

II. EXPERIMENT

The XPS and Auger measurements were performed using Al K_α radiation at the Department of Physics of

Uppsala University, Sweden.[10] The x-ray source consists of a fine-focused high-power electron gun, a water-cooled high-speed rotating anode, and a wide-angle crystal monochromator mounted on a Rowland circle arrangement.

The electron analyzer is based on a hemispherical geometry with a large mean radius (360 mm) and a multichannel detector. An overall energy resolution of about 0.3 eV can be achieved with this system.

Resonant valence-band photoemission spectra at the Cu L_3 threshold and Auger spectra near the Cu L_2 threshold were taken at the soft x-ray beamline 22 at the MAX synchrotron-radiation laboratory in Lund, Sweden. The beamline is equipped with a modified SX-700 plane grating monochromator and a hemispherical electron energy analyzer of 200-mm mean radius with a multichannel detector. Valence-band photoemission spectra at the Cu L_3 edge have been taken with a photon energy resolution and electron energy resolution of about 1.4 and 0.6 eV, respectively. The overall energy resolution of valence-band spectra measured at 100-eV photon energy was of about 0.1 eV. These measurements are described in more detail in Ref. 11.

$Bi_2Sr_2CuO_6$ and $Bi_2Sr_2CaCu_2O_8$ single crystals were glued with conducting silver epoxy to the sample holder. Clean samples were obtained by cleaving *in situ* at a pressure below 10^{-10} Torr, and were kept in this pressure range throughout the measurements. The growth methods of the two samples are described elsewhere.[11,12] The Bi2212 and Bi2201 crystal structures differ in the number of CuO_2 planes. The Bi2212 has a subunit cell containing two CuO_2 planes separated by a Ca layer,[13–15] and the superconducting transition temperature (T_c) is about 90 K. The Bi2201 structure contains no Ca and has only one CuO_2 plane in the subunit cell.[14,15] T_c is about 20 K or lower.

III. THE CHARGE-TRANSFER MODEL AND SPECTROSCOPIC RESULTS

A. The ground state

In this model, successfully applied to many transition-metal compounds,[4,5,16] the system ground state is considered as a mixture of purely ionic configurations $d^n\underline{L}^m$, where $m + (10-n)$ is the number of holes distributed among the ligand orbitals (m) and the d shell ($10-n$), respectively ($\underline{L}$ indicates a hole in one ligand orbital created by a charge transfer to a $3d$ state). This set of electronic configurations can be considered a good base set on which the ground and excited states of correlated systems can be expanded. Early measurements on copper compounds revealed a straightforward connection between the presence of a satellite in the Cu $2p$ photoemission spectra and the valence of the Cu ion.[17,18] By comparing the Cu $2p$ photoemission spectra of CuO and Cu_2O the absence of a satellite in Cu_2O is accompanied by a shift to lower binding energy for the core level, which has been interpreted as the reduction from Cu^{2+} to Cu^+.[17] The same satellite features observed in the case of CuO are present in the spectra measured on copper oxide based

HTS's,[2] showing a dominant divalent behavior of the copper ion. Within this framework the only configurations needed to expand the ground state are $3d^9$ and $3d^{10}\underline{L}$. These two configurations are separated in energy by an amount Δ, defined as

$$\Delta \equiv \langle 3d^{10}\underline{L}|H|3d^{10}\underline{L}\rangle - \langle 3d^9|H|3d^9\rangle , \tag{1}$$

where H is the system Hamiltonian.

Figure 1 shows the energy levels of the configurations that mix in the ground state and in the final states ($N-1$ electrons) of both the core and valence photoemission processes. In a more complete theoretical approach, the δ-like level corresponding to the $3d^{10}\underline{L}$ configuration should be represented by a band of width W centered on that level which originates from the delocalization of the p hole. This is not explicitly considered in the model used in this work, that neglects the translation symmetry of the crystal. The hybridization of these two configurations is given by a transfer integral

$$T \equiv \langle 3d^9|H|3d^{10}\underline{L}\rangle . \tag{2}$$

In order to determine the system ground state for this basis set we evaluate the eigenvalues and eigenvectors of the following 2×2 Hamiltonian:

$$\begin{bmatrix} 0 & T \\ T & \Delta \end{bmatrix} . \tag{3}$$

The origin of the energy scale has been aligned to the $3d^9$ energy. The energy eigenvalues of the Hamiltonian are

$$E_{1,2} = \frac{\Delta}{2} \mp \frac{1}{2}\sqrt{\Delta^2+4T^2} , \tag{4}$$

corresponding to the eigenvectors
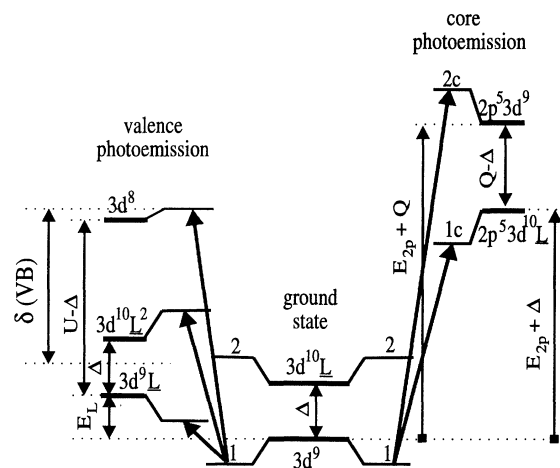
FIG. 1. Energy levels of the configurations that mix in the ground state (center) and in the $N-1$ final states of core (right) and valence-band photoemission processes (left). The arrows represent the projection of the ground state on each of the final $N-1$ electron states. δ(VB) represents the experimental value obtained from Cu $2p \rightarrow 3d$ resonant photoemission (Ref. 11).

$$|1\rangle=\cos\theta|3d^9\rangle-\sin\theta|3d^{10}\underline{L}\rangle$$
$$|2\rangle=\sin\theta|3d^9\rangle+\cos\theta|3d^{10}\underline{L}\rangle \ , \qquad (5)$$

where $|1\rangle$ is the bonding state, $|2\rangle$ the antibonding state, and θ is the hybridization angle, defined by

$$\tan(2\theta)=\frac{2T}{\Delta} \ . \qquad (6)$$

B. Cu 2p XPS

The Cu $2p$ photoemission spectra for the two Bi-Sr-Ca-Cu-O compounds are shown in Fig. 2, where the energy window is limited to the Cu $2p_{3/2}$ region, and an integrated background has been subtracted (for further details, see Sec. IV). The two spectra show a main line and a broad satellite at higher binding energy, both exhibiting a complex structure. The line shape of the satellite has been previously used by van der Laan et al.[4] for copper dihalides to assign this feature to a $2p^5 3d^9$ final state, since it reflects the multiplet splitting deriving from the interaction of one $3d$ hole with a $2p_{3/2}$ hole. As a consequence we assign the main line to a $3d^{10}\underline{L}$ final state, although from our data we can resolve at least three features in it (a, b, and a low binding energy shoulder near the vertical solid lines) and whose explanation is still rather controversial. In recently published works on Ni and Cu oxides[19,20] it has been suggested that the inclusion of more than one single transition-metal ion in the adopted cluster would explain the presence of two features in the main line. Both features are assigned to a configuration having a filled $3d$ shell, but with the tenth electron that screens the core hole coming either from a ligand orbital ($3d^{10}\underline{L}$) or from a neighbor cluster ($3d^{10}$). The screening from a neighbor cluster (metallic screening) is expected to be more efficient than from the ligand. As a consequence the $3d^{10}$ configuration will have a lower binding energy than the $3d^{10}\underline{L}$.

The two solid vertical lines shown in Fig. 2 mark the energies of the Cu L_3 absorption peaks for the two compounds.[21] At the Cu L_3 absorption threshold, in the case of divalent Cu compounds, a $3d^{10}$ final state is reached.
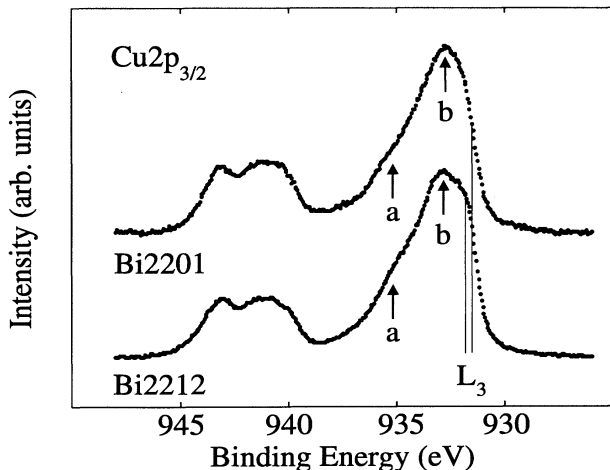
FIG. 2. Cu $2p_{3/2}$ photoemission spectra for $Bi_2Sr_2CaCu_2O_8$ (Bi2212) and $Bi_2Sr_2CuO_6$ (Bi2201). The vertical solid lines (L_3) represent the Cu $2p$ absorption thresholds measured in Ref. 21.

As seen in Fig. 2 the positions of the low binding energy shoulders for the Bi2212 and Bi2201 samples almost correspond to the energy of Cu L_3 absorption peaks. It should also be noted that this low binding energy shoulder is much more intense for Bi2212 than for Bi2201. If this spectral feature is attributed to a metal screening process, a higher intensity for the Bi2212 sample would arise from a higher charge-carrier concentration in Bi2212 than in Bi2201. Since this is expected to be the case, these results could support a nonlocal screening effect as proposed by van Veenendaal and co-workers.[19,20] but the assignment of the other two features, which should reflect a $3d^{10}\underline{L}$ nature, is still an open question.

In this work, adopting an extremely simplified cluster model, we will not take into account these nonlocal effects, in the same way that the multiplet structure of the satellite is neglected. Therefore the splittings between main line and satellite are evaluated as referred to their center of gravity and the intensities are obtained integrating the areas of the two features. As it has been already suggested,[19] this approximation may underestimate the charge-transfer energy.

By a direct comparison between the Cu $2p$ spectra in Fig. 2, it is possible to find out some differences in the satellite to main line intensity ratios and energy separations. These differences reflect the differences in the screening process of the created $2p$ hole. In the Cu $2p$ photoelectron spectroscopy, the creation of a core hole produces a core-hole potential that attracts electrons from the ligand, which results in different weights and energy separations for the two electron configurations as compared to the ground state.

The $2p^5 3d^9$ configuration has a less efficient screening effect on the core hole than the $2p^5 3d^{10}\underline{L}$ one. This difference is quantified as the Coulomb repulsion Q between the $3d$ and $2p$ holes in the $2p^5 3d^9$ configuration.

These screening effects are sketched in the right side of Fig. 1. Here the final-state configuration $2p^5 3d^9$ is represented lifted from the ground-state configuration ($3d^9$) of the energy $E_{2p}+Q$, which is the energy needed to add a core hole to a $3d^9$ configuration. In order to reach the final-state configuration $2p^5 3d^{10}\underline{L}$, an extra energy amount of Δ eV is needed for the charge-transfer process from the ligand. However, this energy is largely regained by a much more efficient screening of the core hole, since the repulsive $2p$-$3d$ Coulomb interaction is not present in this final-state configuration. In this case, with $Q>\Delta$, the $2p^5 3d^{10}\underline{L}$ configuration would have a lower binding energy than the $2p^5 3d^9$ configuration and their energy separation would be $Q-\Delta$, as shown in the figure.

This description of the final-state effect is consistent with the previously mentioned assignment of the main line and the satellite of the Cu $2p$ photoemission spectra in Fig. 2. The energy separation between the main line and the satellite is then equal to $Q-\Delta$ plus the hybridization shifts of the levels due to the mixing of these two final states. The eigenvalues and eigenvectors of the Hamiltonian describing the system excited by the creation of a core hole are obtained by substituting Δ with $\Delta-Q$ in expressions (4)–(6) and by shifting the ener-

gy scale by $E_{2p} + Q$. Thus we obtain

$$(E_{1,2})_c = \frac{\Delta - Q}{2} \mp \frac{1}{2}\sqrt{(\Delta - Q)^2 + 4T^2} + (E_{2p} + Q) , \quad (7)$$

$$|1c\rangle = \cos\phi |3d^9\rangle - \sin\phi |3d^{10}\underline{L}\rangle$$
$$|2c\rangle = \sin\phi |3d^9\rangle + \cos\phi |3d^{10}\underline{L}\rangle , \quad (8)$$

$$\tan(2\phi) = \frac{2T}{\Delta - Q} , \quad (9)$$

where ϕ is the new hybridization angle. As pointed out above, Q is larger than Δ and therefore $\phi > 45° > \theta$ for $T > 0$ and $\theta > 45° > \phi$ for $T < 0$.

Within the framework of the sudden approximation, it is possible to calculate the intensities of the spectral features as the square of the dot product between the initial state and each of the final-state eigenvectors reached after the charge relaxation. As initial state, the sudden approximation considers the ground state with a hole in a Cu $2p$ orbital and with the remaining orbitals unaffected. This means that the same basis set can be used to describe both the ground state and the core-ionized final state.

In this way, we can compare the experimental satellite to main line intensity ratio with

$$\left[\frac{\langle 1|2c\rangle}{\langle 1|1c\rangle} \right]^2 = \tan^2(\phi - \theta) , \quad (10)$$

and the energy splitting between the centers of gravity of these two features, with the separation of the two final-state eigenvalues:

$$E_{2c} - E_{1c} = \sqrt{(\Delta - Q)^2 + 4T^2} . \quad (11)$$

With the hybridization angles in Eq. (10) given as a function of the model parameters Δ, Q, and T, (10) and (11) constitute a system of two equations and three variables. The solution is graphically represented in Fig. 3(a),
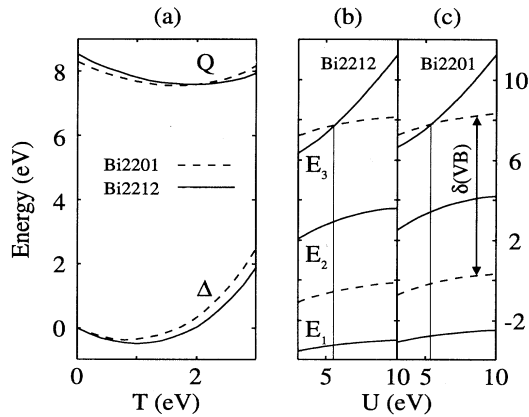
FIG. 3. (a) Q and Δ as a function of T, by using Eqs. (10) and (11), for the two Bi-Sr-Ca-Cu-O samples; (b) eigenvalues of (19) as a function of U with $T = 2.4$ eV and $\Delta = 0.6$ eV for $Bi_2Sr_2CaCu_2O_8$; (c) the same as (b) but for $Bi_2Sr_2CuO_6$ with $T = 2.4$ eV and $\Delta = 1$ eV. The vertical solid lines in (b) and (c) mark the value of U for which the separation between E_3 and a proper average of E_1 and E_2 is equal to the experimental value δ (VB).

where Δ and Q are plotted versus T for the two samples. The solid and broken lines correspond to the values for Bi2212 and Bi2201, respectively.

These plots provide a link between the parameters, but they are not exhaustive for a numerical evaluation of them. In order to achieve this goal, we made use of valence-band photoemission spectroscopy. With this technique a fourth model parameter, the Coulomb repulsion U between the Cu $3d$ valence electrons, is introduced in the model. The final choice of the four parameters consistent with the experimental spectra can be obtained by considering the intensities and splittings of the valence-band configurations as will be discussed below.

C. Valence-band photoemission spectroscopy (Ref. 11)

After the photoemission of a valence electron, the occupation number of the Cu $3d$-O $2p$ hybridized orbitals is reduced by one. This implies that all the electronic configurations that mix in the $N - 1$ electron final states are those which contain two holes distributed between the Cu $3d$ and the O $2p$ orbitals: $3d^8$, $3d^9\underline{L}$, and $3d^{10}\underline{L}^2$. The energy positions of these final-state configurations, as referred to the $3d^9$ energy, are shown in the left side of Fig. 1. The picture is drawn for $\Delta < U$, which has been shown to be the case for late transition-metal oxides.[1,6,9,22] E_L is the energy required to create a ligand hole. The $3d^{10}\underline{L}^2$ state lies at an energy Δ higher than the $3d^9\underline{L}$ state, since these two configurations are connected by a charge-transfer fluctuation that requires the creation of an additional ligand hole and the addition of an extra d electron. The energy separation Δ can thus be written

$$\Delta = E_L + E_d , \quad (12)$$

where E_d is the energy required to add the tenth d electron.

The energy needed for the charge fluctuation $d^9 d^9 \leftrightarrow d^{10} d^8$ defines the parameter U as

$$U \equiv E(3d^{10}) + E(3d^8) - 2E(3d^9) = E(3d^{10}) + E(3d^8) . \quad (13)$$

The energy position of the $3d^8$ final state is then equal to

$$E(3d^8) = U - E(3d^{10}) = U - E_d = U - \Delta + E_L . \quad (14)$$

With the choice of this three configuration basis set, the eigenvectors of the $N - 1$ electron system are

$$|\psi_i\rangle = a_i |3d^9\underline{L}\rangle + b_i |3d^{10}\underline{L}^2\rangle + c_i |3d^8\rangle , \quad (15)$$

while the matrix representation of the Hamiltonian is

$$\begin{bmatrix} E_L & T\sqrt{2} & T\sqrt{2} \\ T\sqrt{2} & E_L + \Delta & 0 \\ T\sqrt{2} & 0 & E_L + U - \Delta \end{bmatrix} . \quad (16)$$

The $\sqrt{2}$ coefficient accounts for the degeneracy of the $3d^9\underline{L}$ final state.[5] Denoting with $|d_i\rangle$ a state obtained starting from a closed Cu $3d$ shell by adding one hole in a $3d$ orbital belonging to the ith irreducible representation (IR) and with $|\underline{L}_j\rangle$ a state with a p hole in a O $2p$ orbital

of the jth IR, the configurations that mix in the photoemission final states can be represented as

$$|3d^8\rangle = |\underline{d}_i\underline{d}_j\rangle \, ,$$

$$|3d^9\underline{L}\rangle = \frac{1}{\sqrt{2}}(|\underline{d}_i\underline{L}_j\rangle + |\underline{d}_j\underline{L}_i\rangle) \, , \qquad (17)$$

$$|3d^{10}\underline{L}^2\rangle = |\underline{L}_i\underline{L}_j\rangle \, .$$

Since Cu $3d$ states can mix only with ligand hole states having the same symmetry, and defining T according to (2) as $\langle \underline{d}_i|H|\underline{L}_i\rangle$, the off-diagonal elements of (16) will be

$$H_{13} = \langle 3d^9\underline{L}|H|3d^8\rangle$$

$$= \frac{1}{\sqrt{2}}(\langle \underline{d}_i\underline{L}_j|H|\underline{d}_j\underline{d}_i\rangle + \langle \underline{d}_j\underline{L}_i|H|\underline{d}_i\underline{d}_j\rangle)$$

$$\cong \sqrt{2}T = H_{31} = H_{12} = H_{21} \, , \qquad (18)$$

while $H_{32} = H_{23} = 0$.

In order to simplify the Hamiltonian we can add to (16) the constant value $\Delta - E_L = E_d$. By doing that we take away the dependence on E_L and obtain

$$\begin{bmatrix} \Delta & T\sqrt{2} & T\sqrt{2} \\ T\sqrt{2} & 2\Delta & 0 \\ T\sqrt{2} & 0 & U \end{bmatrix} \, . \qquad (19)$$

In this way all the eigenvalue energies are rigidly shifted by E_d, while the eigenvectors are not affected.

In this new form the Hamiltonian explicitly depends on the model parameters that define the main charge fluctuations. It is possible to obtain the three eigenvalues of (19) as a function of U for each couple of T and Δ chosen according to the analysis of the Cu $2p$ photoemission spectra.

The solution to this eigenvalue problem can be compared with the valence-band (VB) photoemission spectra for the two compounds. These spectra are already reported and discussed in detail in Ref. 11.

By exploiting resonant photoemission measurements at the Cu L_3 threshold, the enhanced VB satellite at about 12 eV of binding energy has been assigned to a final state with a dominant $3d^8$ contribution, while the structure below the Fermi level originates mainly from the mixing of the $3d^9\underline{L}$ and $3d^{10}\underline{L}^2$ final states.

The energy separation δ(VB) between the peak of the enhanced VB satellite seen on resonance and the center of gravity of the main VB structure seen off resonance, can then be fitted to the energy separation between the higher-energy eigenvalue of (19) and a weighted average of the first two. The result of this analysis is given in the right panels in Fig. 3, where the solid lines of the two plots (b) and (c) represent the three eigenvalues of (19) as a function of U for both the compounds. The broken line at lower energy is an average of the first two eigenvalue curves, while the second broken line is a replica of the first but shifted with the experimental value δ(VB) in order to find the crossing with the third eigenvalue curve.

The choice for the weights of the two lower-energy eigenvalues that mix together results in a clear difference among the solutions of the model.[23] Since *a priori* any choice is somehow arbitrary, we improved the simple

model previously used for other superconducting compounds[2] by developing a computer procedure that iteratively adjusts these weights until a convergence in the numerical solution is found. Having equal weights for the two configurations at the beginning, the program finds the value of U which matches to the experimental value the calculated energy separation between the centroid of the two less bounded eigenvalues and the $3d^8$-like eigenvalue. The eigenvectors of the Hamiltonian are then evaluated corresponding to this value of U, and the projection of the ground state of the N electron system (5) on each of these final-state eigenvectors (15) of the $N-1$ electrons system is calculated, according to

$$I_i = |\langle 1|\psi_i\rangle|^2 = (\cos\theta c_i - \sin\theta a_i)^2 \, . \qquad (20)$$

The spectral intensities for the two low binding energy eigenvectors (I_1 and I_2) given by (20) are then used to evaluate the new weights:

$$w_i = \frac{I_i}{I_1 + I_2} \, , \quad i = 1, 2 \, . \qquad (21)$$

With these new weights the procedure is repeated and the iterations continue until a convergence in the value of U is reached.

Following this procedure, several sets of numerical solutions for the model Hamiltonian parameters can be produced, each set corresponding to a particular couple of input values for T and Δ. For each set of solutions some spectroscopic parameters can also be obtained. For instance the VB satellite intensity is given by (20), while the VB width can be evaluated as the energy separation between the $3d^9\underline{L}$ and $3d^{10}\underline{L}^2$ final-state configurations, which is the energy difference between the first two eigenvalues of (19).

By comparison with the experimental values, the spectroscopic parameters can be used to extract among the several possible sets of solutions the one which best fits together the core and valence-band photoemission data. This will be discussed in detail in Sec. IV. The possibility of using the line shape of the Cu LVV Auger spectrum to derive an additional constrain for the model parameters will be examined in the following section.

D. Auger LVV spectra

Due to the localized nature of the core Cu $2p$ hole, the Cu $L_{23}VV$ spectra of Cu compounds can be used to quantify the amount of energy needed for the localization of two d holes on the same Cu site. The difference between the Cu $2p$ binding energy and the kinetic energy of the Cu LVV main line gives some information about the size of the d-d charge fluctuation energy, U.[24,25]

Moreover, in an early work on copper dihalides,[4] the Cu $L_3M_{45}M_{45}$ spectral line shape has been attributed to different three-hole final-state configurations reached after the Auger decay process. According to this interpretation, the main line of the Auger Cu $L_3M_{45}M_{45}$ spectra [feature B in Fig. 4(a)] could be assigned to a $3d^8\underline{L}$ final-state configuration, reached after the decay from a $\underline{2p}_{3/2}3d^{10}\underline{L}$ intermediate state, while the low kinetic ener-

gy satellite (feature A) could instead be assigned to a $3d^{\prime}$ configuration originating from a $\underline{2p}_{3/2}3d^9$ intermediate state. In this way the energy separation between A and B would give an additional constrain to the model Hamiltonian parameters. Nevertheless, the presence of a Coster-Kronig $L_2L_3M_{45}$ process that precedes the Auger transition has often been used as an argument against the interpretation of the low kinetic energy satellite A as a configuration interaction effect.[1] In this Coster-Kronig process the original $2p_{1/2}$ hole is filled leaving one vacancy in a $2p_{3/2}$ state and one in the valence band. The presence of an extra $3d$ hole in the Auger $L_3M_{45}M_{45}$ decay that follows causes the reduced kinetic energy of the outgoing electron and gives rise to a satellite which, in Auger photoelectron coincidence spectroscopy measurements on Cu metal,[26] has been measured at a kinetic energy 2.5 eV lower than the main line kinetic energy.

In order to shed new light on this matter, we performed photon energy-dependent Cu LVV Auger measurements on the Bi2212 compound. The aim of this study is to compare the spectra taken at photon energy either below or above the Cu L_2 threshold, in order to understand the role of the Coster-Kronig decay in the spectral shape. The results of this analysis are shown in Fig. 4.

Each Cu $L_3M_{45}M_{45}$ Auger spectrum shown has been measured at a different photon energy: 1486.6, 974, and 947 eV for spectra (a), (b), and (c), respectively. Three main features can be identified in curve (a): a main line marked with B, and two satellites A and C, at lower and higher kinetic energy, respectively. Curves (b) and (c) have been measured by using tunable synchrotron-radiation light. The choice of the photon energies above and below the L_2 threshold (974 and 947 eV, respectively) has been made in such a way as to minimize the overlap between the Auger and the photoemission signal. However, since it is impossible to avoid some overlap with the strong Bi $5d$ photoemission signal, we also measured a spectrum at a photon energy lower than the L_3

FIG. 4. Cu $L_3M_{45}M_{45}$ Auger transition for $Bi_2Sr_2CaCu_2O_8$ at three different photon energies: (a) 1486.6 eV, (b) 974 eV, and (c) 947 eV.

threshold (925 eV), which was used for background subtraction from the spectra taken at 947- and 974-eV photon energy. In this way, the photoemission signal can be suppressed, and curves (b) and (c) are produced. The good agreement between curves (a) and (b) proves the reliability of this procedure.

As curve (c) clearly shows, below the L_2 threshold the low kinetic energy satellite A is suppressed. This clearly manifests the Coster-Kronig nature of the low kinetic energy satellite.

IV. MODEL RESULTS AND DISCUSSION

All the experimental values used as input parameters in the model are summarized in Table I. In this table we have collected the values for the two Bi-Sr-Ca-Cu-O compounds and the values for CuO taken from literature.[1,7] We have applied the same analysis also to CuO, since it can be considered as a model compound for the copper oxide based HTS's. Moreover, a comparison between our results for CuO and those obtained in other works is a useful test of the consistency among the different theoretical methods.

One effect that should not be neglected in order to avoid misleading conclusions is the presence of a weak Bi $4s$ emission overlapping the Cu $2p_{3/2}$ signal in the Bi-based superconductors. The atomic cross section for Bi $4s$ photoemission is about 10% of the Cu $2p$ cross section at Al K_α photon energy.[27] Moreover these $4s$ states give rise to a very broad feature [full width at half maximum (FWHM) $\cong 9$ eV] as measured on oxidized Bi.[28] However, the different ratio between Bi and Cu concentration in the two samples (1:1 in Bi2212 and 2:1 in Bi2201), causes different effects on the two. Since the energy position of the Bi $4s$ emission peak is closer to the satellite than to the main line energy, this could contribute to a higher satellite to main line intensity ratio in the Bi2201 sample. On the other hand the intensity ratios evaluated using the Cu $2p_{1/2}$ spin orbit term may be influenced by the presence of the oxygen KLL Auger emission which could distort the high binding-energy tail of the satellite. We decided to correct the Cu $2p_{3/2}$ spectra by subtracting a curve that simulates the Bi $4s$ emission. This curve is given by a Lorentzian function with a FWHM of 9 eV and centered at a binding energy (BE) of 940.3 eV. This value is given by the metallic Bi $4s$ BE (939 eV),[29] plus a chemical shift equal to the shift measured on the Bi $4f$ doublets of our two samples as compared to the metallic Bi $4f$. The curve peak height has been deduced from the comparison between the Bi $4s$ and Bi $4p_{3/2}$ peak heights in the data published for Bi metal[30] and between the Bi
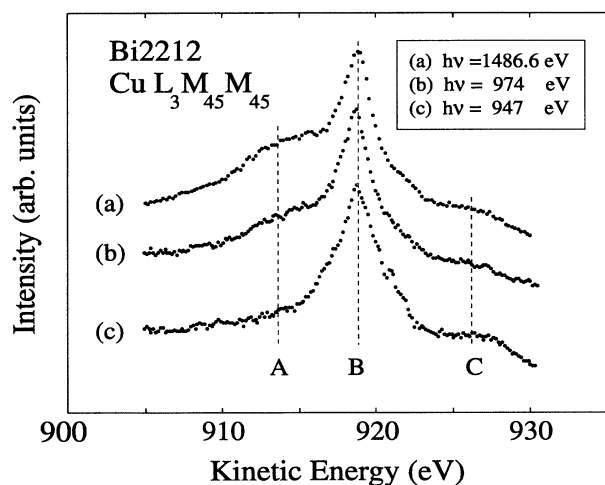
TABLE I. Experimental values for the Bi-Sr-Ca-Cu-O compounds and for CuO from Refs. 1 and 7 (all the energy values are given in eV).

Samples	Is/Im (XPS)	Is/Im^* (XPS)	δ (XPS)	δ (VB)
Bi2212	0.4	0.37	8.55	8.3
Bi2201	0.48	0.42	8.3	8
CuO	0.55 (Ref. 1)		8.7 (Ref. 1)	9.2 (Ref. 7)

$4p_{3/2}$ and Cu $2p_{3/2}$ main line heights in wide-energy-range spectra for our two samples. The spectra shown in Fig. 2 are the result of both the subtraction of an integrated background and of the simulated Bi 4s emission. The consequence is a reduction of about 10% in the satellite to main line intensity ratios for the two samples (Table I, second column).[31]

For the satellite to main line intensity ratios, both numbers obtained from the background subtracted Cu $2p_{3/2}$ spectra [Is/Im (XPS)] and those from the Bi 4s emission corrected spectra [Is/Im^* (XPS)] are given in Table I. The latter ones are those that have been used. δ(XPS) measures the splitting between the $2p3d^{10}\underline{L}$ configuration and the $2p3d^9$ in the core photoemission spectra. δ(VB) is obtained from valence-band resonant photoemission measurements and corresponds to the energy splitting between the intensity maximum of the valence-band satellite ($3d^8$) taken on resonance and the center of gravity of the VB main feature, off resonance. The on-resonance measurements have been taken at the Cu $2p \rightarrow 3d$ threshold in our work and at the Cu $3p \rightarrow 3d$ for CuO.[7]

Table II collects the results of our analysis by using the values given by Table I for Bi2212, Bi2201, and CuO, to be compared with the published results for CuO,[1,7] and for La-Sr-Cu-O and Y-Ba-Cu-O superconductors.[2] The solution that we evaluate for CuO is obtained by fixing the value of T to 2.5 eV, in agreement with values from literature. Our U value is greater than the ones given in Refs. 2 and 7, while Δ is in between the solutions of Refs. 1 and 7. It should be pointed out that although our method is, in principle, the same as used by Shen and co-workers,[2] the numerical solutions are different. These differences come partially from slightly different experimental value and partially from the different weights for the two less bounded eigenvalues of (19) applied to fit the valence-band photoemission data, which are iteratively adjusted in the present analysis as described above (see Ref. 23). Moreover the small difference in Δ between our solution and the one given in Ref. 1 comes from a different choice of the boundary conditions. The solution in Ref. 1 corresponds to a fixed value of 9 eV for Q, while we used an extra boundary condition from the valence-band spectra.[7]

TABLE II. Solutions for the model parameters of Bi-Sr-Ca-Cu-O compounds, CuO, La-Sr-Cu-O, and Y-Ba-Cu-O compounds. The values are either derived by using the model described in this work, or taken from literature in the case of CuO, La-Sr-Cu-O, and Y-Ba-Cu-O (Refs. 1, 2, and 7).

Samples	T (eV)	Δ (eV)	U (eV)	Q (eV)
Bi2212	2.4	0.6	5.6	7.6
Bi2201	2.4	1	5.4	7.7
CuO	2.5	1.6	8.2	8.7
CuO (Ref. 7)	2.5	1.75	7.76	
CuO (Ref. 1)	2.5	1.55		9
CuO (Ref. 2)	2.4	1	7.3	8.4
La$_2$CuO$_4$ (Ref. 2)	2.3	0.3	6.5	7.4
La$_{1.8}$Sr$_{0.2}$CuO$_4$ (Ref. 2)	2.4	0.3	6.1	7.8
YBa$_2$Cu$_3$O$_7$ (Ref. 2)	2.5	0.5	6.5	7.8

The criterion used to choose the best set of T, Δ, U, and Q values for Bi2212 and Bi2201 was to compare the calculated VB width and VB satellite/main line intensity ratios with the experiment. As a matter of fact by increasing T and Δ, which are mutually linked by the core photoemission data, the calculated VB width increases, while the satellite to main line intensity ratio decreases. Our solution represents the best trade off, since high T and Δ values are needed to reproduce the low VB satellite intensity, while lower T and Δ values would better fit the VB width with the experiment.

Moreover in this way the T values for the Bi2212 and Bi2201 are the same, and close to values given for CuO. This is consistent with the fact that the Cu-O bond length in the CuO$_2$ planes of Bi-Sr-Ca-Cu-O compounds is the same for Bi2212 and Bi2201 (1.91 Å),[15] and very close to that for CuO (1.95 Å) (Ref. 1, and references therein).

The U values for the Bi-Sr-Ca-Cu-O compounds are smaller than the solutions given for different CuO-based HTS's (Refs. 2 and 23), while Δ seems to be the most compound dependent parameter. This has been previously observed for different late transition-metal dihalides,[32] where U and T remained constant when changing the anion (halide), while Δ strongly depended on the anion electronegativity (higher for higher electronegativity).

According to our results, Δ could also reflect the different O cluster that surrounds the Cu atom, since in the Bi2201 and Bi2212 samples we have a CuO$_6$ octahedron and a CuO$_5$ tetrahedron, respectively.

Within the framework given by Zaanen, Sawatzky, and Allen (ZSA),[9] it is possible to use the model Hamiltonian parameters U, T, and Δ to explain a metallic or insulating behavior of the studied compounds. Both the Bi-Sr-Ca-Cu-O samples exhibit a small spectral intensity at the Fermi level, particularly evident for the Bi2212 sample. In the same time the solutions do not differ significantly from the values of CuO, which is a well known semiconductor belonging to the charge-transfer regime of the ZSA phase diagram and having a measured optical band gap of 1.4 eV.[33] For other copper oxide superconductors, belonging to the Y-Ba-Cu-O or La-Sr-Cu-O families, a band gap of about 1 eV has been calculated in a cluster-configuration-interaction approach,[2] and the values for Δ and U identify them as charge-transfer semiconductors.

The energy gap can be calculated as the minimum energy required to remove one electron from the ground state of the system plus the minimum energy to add one. Within the framework of the ZSA model, without considering the hybridization shifts of the energy levels in the electron removal and electron addition systems, the energy gap is given by the minimum value between the two main charge fluctuation parameters: Δ and U. When considering the hybridizations effects, for a charge-transfer insulator, we obtain

$$E_g = \Delta^* + 2\delta^n - \delta^{n-1} - \delta^{n+1} , \qquad (22)$$

where δ^k is the hybridization shift for a system with k 3d electrons. In (22) the O 2p bandwidth of the charge transferred state is completely neglected (i.e., $3d^{10}\underline{L}$ for the copper oxide ground state). This means that the Δ^*

value to be used in (22) should be the minimum excitation energy required to reach the bottom of the O $2p$ band centered on the $3d^{n+1}\underline{L}$ level starting from the $3d^n$ ground state. If on the contrary Δ is referred to the center instead of the bottom of the O $2p$ band, it is necessary to subtract $W/2$ from (22), where W is the full O $2p$ bandwidth. The present work is based on a spectroscopic approach to determine Δ. It is most plausible that it is the minimum excitation energy that gives the well screened Cu $2\underline{p}3d^{10}\underline{L}$ final state. This means that throughout this work we have implicitly used Δ^* and that the following relation should hold between the Δ^* value derived from the present Cu $2p$ XPS measurements and the definition of Δ to be used in *ab initio* calculation:

$$\Delta^* = \Delta - W/2 \ , \tag{23}$$

as already pointed out by Eskes and Sawatzky.[34]

In the case of divalent copper compounds $n = 9$ and $\delta^{n+1} = 0$, since there is only one possible final-state configuration after the addition of one electron. The hybridization shift in the ground state can be evaluated easily using the 2×2 Hamiltonian (3) as

$$\delta^9 = \frac{1}{2}\sqrt{\Delta^2 + 4T^2} - \frac{\Delta}{2} \ . \tag{24}$$

δ^8 is equal to the energy difference between the H_{11} element of (19), Δ, and the lowest energy eigenvalue corresponding to a final-state eigenvector originated from the hybridization of the $3d^9\underline{L}$ configuration with the other two configurations in the $N-1$ system.

Table III shows the calculated energy gaps for the two Bi-Sr-Ca-Cu-O compounds and for the CuO, using the values from Table II, and the band gaps calculated for other copper oxide HTS's quoting the values from literature.[2] The hybridization shifts calculated for the ground state (δ^9) and for the valence-band photoemission final state (δ^8) are also shown. It is noteworthy that the band gap of CuO, calculated by means of our simple method, is close to the experimental value (1.4 eV).

We evaluate a band gap of about 1 eV for both the Bi-Sr-Ca-Cu-O compounds (1 eV and 1.1 eV for Bi2212 and Bi2201, respectively), which place them in the charge-transfer semiconductor region of the ZSA diagram. This is represented in the phase diagram of Fig. 5, where curves at constant energy gap are plotted as a function of

TABLE III. Hybridization shifts and energy gaps calculated for the Bi-Sr-Ca-Cu-O compounds and CuO. The energy gap and hybridization shifts for CuO are also calculated using the parameters given in Ref. 7. The energy gaps for the La-Sr-Cu-O and Y-Ba-Cu-O and CuO samples given in Ref. 2 are quoted.

Samples	δ^9 (eV)	δ^8 (eV)	E_g (eV)
Bi2212	2.1	3.85	1
Bi2201	1.95	3.8	1.1
CuO	1.8	3.6	1.65
CuO (Ref. 7)	1.75	3.6	1.7
CuO (Ref. 2)	1.95	3.65	1.3
La$_2$CuO$_4$ (Ref. 2)	2.15	3.7	1
La$_{1.8}$Sr$_{0.2}$CuO$_4$ (Ref. 2)	2.25	3.9	0.9
YBa$_2$Cu$_3$O$_7$ (Ref. 2)	2.25	4	1.1
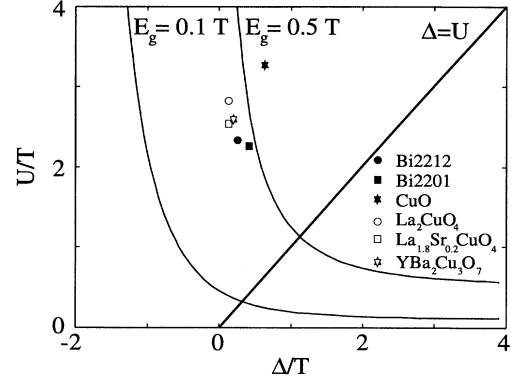
FIG. 5. ZSA phase diagram for copper compounds ($n = 9$), obtained by means of Eq. (22). The two curves shown in the diagram correspond to $E_g = 0.1$ T, and to $E_g = 0.5$ T. The points representative of the La-Sr-Cu-O and Y-Ba-Cu-O compounds have been placed using values from Ref. 2 while for CuO we evaluated the parameters by using the experimental values of Refs. 1 and 7.

U/T and Δ/T for the copper compounds by using formulas (22) and (24). The points shown in the figure correspond to the values for Bi2212, Bi2201, CuO (our result), and for other copper oxide HTS's according to the values given by Shen *et al.*[2] It should be noticed that all the points corresponding to the HTS are grouped in a narrow region of the diagram which lies close to the CuO point.

The observed metallic behavior for Bi2212 and Bi2201, in spite of the calculated energy gaps, can be explained within the framework of doping-induced states in the semiconductor gap. The overlap of these states can create a band partially superimposed on the valence band, as has been suggested by Takahashi and co-workers[35,36] in the analysis of high-energy spectroscopy on Bi-Sr-Ca-Cu-O compounds with different amount of hole doping.

Another experimental indication that the metallic conductivity is due to doping is provided by photoemission and x-ray-absorption spectroscopy of Cs adsorption on Bi$_2$Sr$_2$CaCu$_2$O$_8$ samples.[37] According to this work, by the evaporation of small amounts of Cs on a cleaved Bi$_2$Sr$_2$CaCu$_2$O$_8$ surface, states at and near the Fermi level are depleted. This result is also in support of a doped charge-transfer semiconductor.

On evaluating the constant band gap energy curves traced in Fig. 5, no solution corresponding to $E_g = 0$ was found. This means that, within our simple model suitable for divalent copper compounds with a ground state expanded on $3d^9$ and $3d^{10}\underline{L}$ configurations, there is no solution corresponding to a metallic behavior. This is not in contradiction to the case of copper sulphides and selenides, which are well known metals, since copper proves to be monovalent in these compounds,[38,39] meaning that the $3d^9$ configuration is not the lowest lying ionic configuration.

V. CONCLUSIONS

In this work we applied a simplified charge-transfer model to the study of Bi2212 and Bi2201 superconduc-

tors. This approach allowed us to evaluate the main model Hamiltonian parameters and to discuss the metallic behavior of these compounds. The comparison of the parameters evaluated for other copper oxide based HTS's shows that these values do not differ much in the different compounds.

The results of our analysis suggest that these compounds should be considered as doped charged-transfer semiconductors, with a calculated gap of about 1 eV. This value, nearly the same as for the gaps of other copper oxide based HTS's calculated with a similar approach, should correspond to the gap of a completely undoped mother compound.

The clearest difference in our comparison between Bi2212 and Bi2201 is found for the charge-transfer parameter Δ, which is larger in Bi2201 than in Bi2212. Finally, a clear evidence of a Coster-Kronig transition in the Cu LVV spectra is given, which discards the assignment of the low kinetic energy satellite to a final-state configuration effect.

ACKNOWLEDGMENTS

[1] J Ghijsen, L. H. Tjeng, J. van Elp, H. Eskes, J. Westerink, G. A. Sawatzky, and M. T. Czyzyk, Phys. Rev. B **38**, 11 322 (1988).

[2] Z. X. Shen, J. W. Allen, J. J. Yeh, J. S. Kang, W. Ellis, W. Spicer, I. Lindau, M. B. Maple, Y. D. Dalichaouch, M. S. Torikachvili, J. Z. Sun, and T. H. Geballe, Phys. Rev. B **36**, 8414 (1987).

[3] S. Larsson, Chem. Phys. Lett. **32**, 401 (1975); **40**, 362 (1976); S. Larsson and M. Braga, ibid. **48**, 596 (1977).

[4] G. van der Laan, C. Westra, C. Haas, and G A. Sawatzky, Phys. Rev. B **23**, 4369 (1981).

[5] J. Zaanen, C. Westra, and G. A. Sawatzky, Phys. Rev. B **33**, 8060 (1986).

[6] A. Fujimori and F. Minami, Phys. Rev. B **30**, 957 (1984).

[7] H. Eskes, L. H. Tjeng, and G. A. Sawatzky, Phys. Rev. B **41**, 288 (1990).

[8] A. Fujimori, E. Takayama-Muromachi, Y. Uchida, and B. Okai, Phys. Rev. B **35**, 8814 (1987); A. Fujimori, S. Takekawa, E. Takayama-Muromachi, Y. Uchida, A. Ono, T. Takahashi, Y. Okabe, and H. Katayama-Yoshida, Phys. Rev. B **39**, 2255 (1989).

[9] J. Zaanen, G. A. Sawatzky, and J. W. Allen, Phys. Rev. Lett. **55**, 418 (1985); J. Zaanen and G. A. Sawatzky, Can. J. Phys. **65**, 1262 (1987).

[10] For a detailed description of the experimental apparatus, see for example: A. Nilsson and N. Mårtensson, Phys. Rev. B **40**, 10 249 (1989).

[11] M. Qvarford, J. F. van Acker, J. N. Andersen, R. Nyholm, I. Lindau, G. Chiaia, E. Lundgren, S. Söderholm, U. O. Karlsson, S. A. Flodström, and L. Leonyuk, Phys. Rev. B **51**, 410 (1995).

[12] D. B. Mitzi, L. W. Lombardo, A. Kapitulnik, S. S. Laderman, and R. D. Jacowitz, Phys. Rev. B **41**, 6564 (1990).

[13] S. A. Sunshine, T. Seigrist, L.F. Schneemeyer, D. W. Murphy, R. J. Cava, B. Batlogg, R. B. van Dover, R. M. Fleming, S. H. Glarum, S. Nakahara, R. Farrow, J. J. Krajewski, S. M. Zahurak, J. V. Waszczak, J. H. Marshall, P. Marsh, L. W. Rupp, Jr., and W. F. Peck, Phys. Rev. B **38**, 893 (1988).

[14] J. B. Torrance, Y. Tokura, S. J. LaPlaca, T C. Huang, R. J. Savoy, and A. I. Nazzal, Solid State Commun. **66**, 703 (1988).

[15] J. M. Tarascon, W. R. McKinnon, P. Barboux, D. M. Hwang, B. G. Bagley, L. H. Greene, G. W. Hull, Y. LePage, N. Stoffel, and M. Giroud, Phys. Rev. B **38**, 8885 (1988).

[16] G. Lee and S. J. Oh, Phys. Rev. B **43**, 14 674 (1991).

[17] A. Rosencwaig and G. K. Wertheim, J. Electron. Spectrosc. Relat. Phenom. **1**, 493 (1972).

[18] K. S. Kim, J. Electron. Spectrosc. Relat. Phenom. **3**, 217 (1974).

[19] M. A. van Veenendaal and G. A. Sawatzky, Phys. Rev. Lett. **70**, 2459 (1993).

[20] M. A. van Veenendaal, H. Eskes, and G. A. Sawatzky, Phys. Rev. B **47**, 11 462 (1993).

[21] M. Qvarford, N. L. Saini, J. N. Andersen, R. Nyholm, E. Lundgren, I. Lindau, J. F. van Acker, L. Leonyuk, S. Söderholm, and S. A. Flodström, Physica C **214**, 119 (1993).

[22] G.A. Sawatzky and J. W. Allen, Phys. Rev. Lett. **53**, 2339 (1984).

[23] E.g., for the Bi2212 compound, our solutions for the model parameters are $T = 2.4$ eV, $\Delta = 0.6$ eV, and $U = 5.6$ eV, corresponding to the following weights for the first two eigenvalues of Eq. (19): $w_1 = 0.56$ and $w_2 = 0.44$. Using the same values for T and Δ, but fixing $w_1 = w_2 = 0.5$ as in Ref. 2, the solution for U would be $U = 6.3$ eV.

[24] G. A. Sawatzky, in Auger Spectroscopy and Electronic Structure, edited by G. Cubiotti, G. Mondio, and K. Wandelt, Springer Series in Surface Science, Vol. 18 (Springer-Verlag, Berlin, 1989), p. 2.

[25] J. C. Fuggle, P. J.Weijs, R. Schoorl, G. A. Sawatzky, J. Fink, N. Nüker, P. J. Durham, and W. M. Temmerman, Phys. Rev. B **37**, 123 (1988).

[26] H. W. Haak, G. A. Sawatzky, and T. D. Thomas, Phys. Rev. Lett. **41**, 1825 (1978).

[27] J. J. Yeh and I. Lindau, At. Data Nucl. Data Tables **32**, 1 (1985).

[28] D. M. Hill, H. M. Meyer, J. H. Weaver, C. F. Gallo, and K. C. Goretta, Phys. Rev. B **38**, 11 331 (1988).

[29] J. C. Fuggle and N. Mårtensson, J. Electron. Spectrosc. Relat. Phenom. **21**, 275 (1980).

[30] C. D. Wagner, W. M. Riggs, L. E. Davis, J. F. Moulder, and G. E. Muilenberg (editor), Handbook of X-Ray Photoelectron Spectroscopy, Perkin-Elmer Co., Physical Electronics Division (1979).

[31] These numbers are nearly the same as those evaluated for the Cu $2p_{1/2}$ term, supporting the performed corrections.

[32] J. Park, S. Ryu, M. Han, and S. J. Oh, Phys. Rev. B **37**, 10 867 (1988).

[33]F. P. Koffyberg and F. A. Benko, J. Appl. Phys. **53**, 1173 (1982).

[34]H. Eskes and G. A. Sawatzky, Phys. Rev. Lett. **61**, 1415 (1988); see Ref. 23.

[35]T. Takahashi, in *Strong Correlation and Superconductivity*, edited by H. Fukuyama, S. Maekawa, and A. P. Malozemoff, Springer Series in Solid-State Sciences, Vol. 89 (Springer-Verlag, Berlin, 1989), p. 311.

[36]T. Takahashi, T. Watanabe, T. Kusunoki, and H. Katayama-Yoshida, J. Phys. Chem. Solids **52**, 1427 (1991).

[37]S. Söderholm, M. Qvarford, H. Bernhoff, J. N. Andersen, E. Lundgren, R. Nyholm, U. O. Karlsson, I. Lindau, and S. A. Flodström (unpublished).

[38]J. C. W. Folmer and F. Jellinek, J. Less Common Met. **76**, 153 (1980).

[39]M. Romand, M. Roubin, and J. P. Deloume, J. Electron. Spectrosc. Relat. Phenom. **21**, 229 (1978).